Virtual sensing of wheel direction from redundant sensors in aircraft ground-steering systems

Mattia Dal Borgo · **Stephen J Elliott** · **Maryam Ghandchi Tehrani** · **Ian M Stothers**

Abstract Many safety-critical control systems use multiple redundant sensors to estimate the same controlled signal. If the sensors were to operate perfectly, only a subset of them would need to be used for the estimation. In practice, however, the sensors are subject to uncertainty, minor or major faults and their operation may be nonlinear. It is thus important to reliably estimate the controlled signal under these conditions, and also to assess the degree of confidence with which each sensor should be treated. An example of such a control system is the ground-steering control system of an aircraft nose landing gear. A virtual sensing technique is commonly employed, which estimates the steering angle using the measurements of multiple remote displacement sensors. The wheel position is then calculated as a nonlinear function of these sensor outputs.

This paper describes how a digital twin of the ground-steering system, in which the effects of uncertainties and faults can be systematically analysed and studied, is used to assess the accuracy and integrity of the steering angle estimation for a number of different estimation algorithms. Two of these algorithms are based on a least-squares approach, while another is a soft-computing technique based on fuzzy logic. These methods are investigated for several scenarios where model uncertainty, measurement noise and sensor faults are included. It is shown that the soft-computing approach is more robust than the least squares based methods under these conditions.

Mattia Dal Borgo · Stephen J Elliott · Maryam Ghandchi Tehrani
Institute of Sound and Vibration Research, University of Southampton, SO17 1BJ Southampton, United Kingdom
E-mail: mattia.dalborgo@kuleuven.be
https://orcid.org/0000-0003-4263-0513
Present address of Mattia Dal Borgo:
Department of Mechanical Engineering, KU Leuven, 3001 Leuven, Belgium;
DMMS Lab, Flanders Make, 3001 Leuven, Belgium

Ian M Stothers
Ultra Electronics Precision Control Systems, St Johns Innovation Park, CB4 0DS Cambridge, United Kingdom

1 Introduction

The ground-steering system is a part of the nose landing gear, which is fundamental to an aircraft's safety. A block diagram of the control loop for the ground-steering system is shown in figure 1.
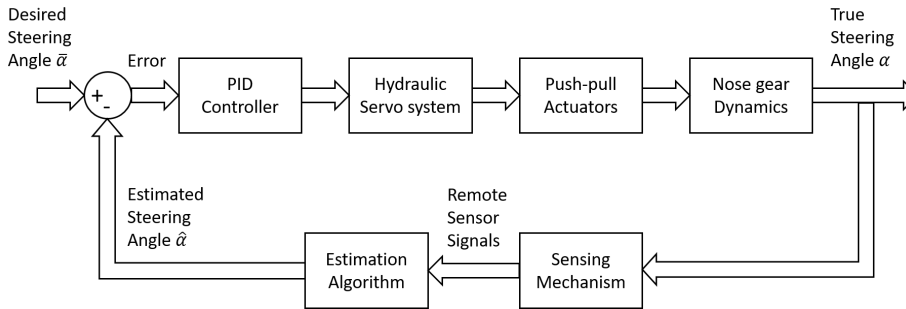

Fig. 1 Ground-steering system feedback control loop.

The nose wheels can be turned by the rudder pedal or by a bar in the cockpit, or by a combination of both. A control law, usually a PID, is then applied on the error signal between the desired steering angle and the actual steering angle. A power-assist system is usually in place to help the pilot action using either electric or hydraulic actuators, which will then turn the nose gear [1–3]. The wheel direction, or steering angle, is commonly not measured directly, with an angular sensor, instead it is estimated using remote linear sensors. Usually, an aircraft nose gear is equipped with a linkage mechanism consisting of multiple linear variable displacement transducers (LVDTs) that are used for this purpose. This is followed by an estimation algorithm that calculates the estimate of the wheel position based on the LVDT outputs, using, in most cases, a majority voting approach. The estimate of the actual steering angle is then fed back to the controller in figure 1 closing the loop.

If the sensors were to operate perfectly, only a subset of them would need to be used for the estimation. However, the internal model of the virtual sensor arrangement might be uncertain, the measurements might be affected by noise and the sensors might be subject to potential faults. So, in practice, the redundant sensor outputs are different from each other. Thus, the research question is how to reliably estimate the controlled signal under these conditions? But also how to assess the integrity of the estimation, hence the trust in the final estimate?

Preliminary work on this topic was presented by the authors in [4,5], where the nonlinear relationship between the steering angle and the sensor signals was first derived and the propagation of both measurement and model uncertainties were investigated. However, these studies lack the derivation of a closed-form solution to determine the possible steering angle values given a sensor measurement, as well as clear and straightforward formulations of the estimation algorithms, the detection of faults and the integrity index, which form the novelty presented in this paper.

This paper presents the development of an "observational" digital twin [6] of an aircraft's ground-steering system sensing mechanism in which the unknown inputs such as uncertainties and faults are included to systematically analyse and test virtual sensing algorithms that are used to estimate the nose wheels direction. Three state estimation algorithms are discussed and their performance in estimating the steering angle is tested under several scenarios including model uncertainty, measurement noise and sensor faults.

The first two approaches are based on the least-squares (LS) method, which are often used for overdetermined problems. Although LS estimators provide good accuracy in presence of uncertainty, it has been observed that they are more difficult to manage when both uncertainties and potential faults are present [5]. The third approach is a soft-computing (S-C) method that makes use of fuzzy logic, which reportedly has been shown to be robust in overdetermined problems under these conditions [7, 8]. The S-C method comprises two parallel algorithms, or modules. The soft-voter module, which calculates the final estimate at each time step; and the decision module, which calculates the overall level of trust in the estimate and detects faulty sensors.

It is a difficult task to distinguish between uncertainties and faults, but the distinction is important since faults, which are unauthorised deviations of at least one characteristic property of the system from acceptable or standard conditions [9], should be flagged up for maintenance. Various sources of uncertainty may disturb diagnosis accuracy, since the model of the system is not a perfect reflection of reality. The existence of measurement noise, model uncertainty, and un-modelled disturbances should be taken into account during design of the virtual sensor. A fault is first flagged up using fault detection and isolation (FDI) techniques, then the control law could be modified to try to compensate for the fault occurrence using fault tolerant control (FTC) methods, a process also known as reconfiguration. Fault diagnosis typically provide a Boolean decision on whether faults have occurred, but an adequate tuning of an FDI procedure should lead to a satisfactory trade-off between minimizing the rates of non-detection (missing a fault) and false-alarm (raising an alarm in fault-free condition). Table 4 in [9] proposes a classification of FDI approaches according to their aerospace applications, from a collection of more than 100 papers. Due to the safety-critical condition of the application presented in this paper, it is important that the FDI provides a high detection rate but that the virtual sensor still guarantees an accurate and smooth steering angle estimate to feed back to the pilot.

The final target of this research is a ground-steering control system that guarantees both the smoothness and predictability of the controlled signal that is fed back to the pilot as they are steering the aircraft on the ground, while being aware on the level of trust they should give to the estimated steering angle, hence the feedback signal.

The paper is organized as follows. The development of the digital twin of the ground-steering system sensing mechanism is presented in section 2, where the nonlinear relationship between the sensor outputs and the steering angle estimates is discussed. For briefness, this will be called as the digital twin of the ground-steering system throughout the rest of the paper. The least squares estimation methods are then introduced in section 3, whereas the soft-computing method is described in section 4. The results of a comparison of the performance of the estimation algorithms in terms of estimation accuracy and integrity when the digital twin is affected by model uncertainty, sensor noise and potential sensor faults, are presented in section 5. The conclusions are summarised in section 6.

2 Problem formulation

In this application, four LVDT sensors are arranged to monitor the nose gear direction, which is calculated based on the nonlinear geometry of the sensor alignment. If the sensors were ideal, only a subset of them would need to be used for the estimation. In practice, however, each sensor is subject to uncertainty, minor (short-term) and major (long-term) faults and there is also ambiguity associated with the estimate of the steering angle because of the geometric nonlinearity. The redundant sensor outputs are thus different from each other, and it is important to not only reliably estimate the controlled signal under these conditions, but also to assess the degree of confidence with which the estimate should be treated. This section presents the development of an observational digital twin of the ground-steering system, in which the effect of nonlinearities, uncertainties, disturbances and faults can be systematically analysed.

The process of estimation can be summarised by the block diagram in figure 2, where α represents the true steering angle, $\hat{\alpha}$ is the estimate of the actual steering angle provided by the estimation algorithm, together with an integrity level, and d_{L1}, d_{L2}, d_{R1}, d_{R2} are the outputs of the 4 LVDTs, which are affected by uncertainties and faults.
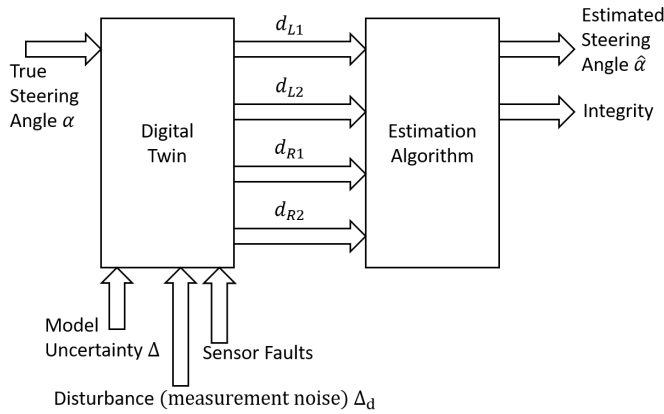

Fig. 2 The digital twin of the ground-steering system sensing mechanism can be used to analyse the effect of uncertainties, disturbances and faults on both the steering angle estimate and the integrity of the estimation.

The estimation process shown in figure 2 is organised with the following elements,

1. α: true steering angle.
2. Digital twin: inputs = $\{Kinematics,\ \alpha\}$, outputs = $\{d_{L1}, d_{L2}, d_{R1}, d_{R2}\}$. Additional (unknown) inputs are:
     Uncertainties: small deviations from true value in the model parameters (a, b, l, γ).
     Disturbances: small deviations from true value in the sensor outputs (d_{L1}, d_{L2}, d_{R1}, d_{R2}).
     Sensor faults: unauthorised deviations from nominal behaviour or complete failures. Common generic sensor faults include: bias, drift, scaling, signal loss and signal lock.

3. Estimator: inputs $= \{Kinematics, \ d_{L1}, d_{L2}, d_{R1}, d_{R2}\}$, outputs $= \{\hat{\alpha}, \ integrity\}$.

   In an ideal case of multiple redundancy, majority voting could be used to estimate the true steering angle and hence any sensor faults, but in practice this is not possible since the sensor outputs are subject to uncertainty and hence the faults may not be obvious. In this paper, three estimation algorithms are presented, two of which are based on a least squares method while the other relies on a fuzzy logic approach.

4. $\hat{\alpha}$: Estimated steering angle; Integrity: level of trust in the estimation.

There are a number of requirements that have been set for the development of both the digital twin and the virtual sensor:

– The estimation algorithm must work using the outputs from the current time step only. This is usually referred as a snapshot scheme, which has the advantage over averaging or filter schemes of not relying on questionable assumptions on how the estimator attained its current state.
– The final estimate must remain smooth at all times, even when a sensor fails abruptly.

Also, it is assumed that a fault occurrence affects only one sensor at a time.

A model of the ground-steering system is shown in figure 3(a), where the coordinates of the linkages have been selected according to the study in [10] and are given in table 1. The two links that rotate around the central pivotal point are fixed in length, while the other links are extensible and their positions are measured by the left and right LVDT sensors.

Table 1 Geometric model parameters for the ground-steering mechanism shown in figure 3, as used in the simulations.

Parameter	Value	Units
e	200	mm
l	153	mm
η	44	[deg]
γ	26	[deg]

A kinematic analysis of position is carried out in order to understand the relationship between the wheel direction and the displacement of the LVDT sensors. The formulation of the forward problem, which determines (d_{Li}, d_{Ri}) given a known steering angle α, has already been presented in [4] and is recalled here for the purpose of introducing the variables. The kinematic analysis is solved by dividing the ground-steering system into elementary triangles, as shown in figures 3(b), 3(c) and 3(d), where each vector $\mathbf{z}_i$ has modulus z_i and direction θ_i, assuming that anticlockwise angles are positive starting from the x-axis.

The closure equation of the left arm shown in figure 3(b) is given by,

$$\mathbf{z}_1 + \mathbf{z}_2 + \mathbf{z}_3 = \mathbf{0}, \tag{1}$$

which can be rewritten as,

$$\begin{cases} z_1 \cos(\theta_1) + z_2 \cos(\theta_2) + z_3 \cos(\theta_3) = 0 & \text{(2a)} \\ z_1 \sin(\theta_1) + z_2 \sin(\theta_2) + z_3 \sin(\theta_3) = 0 & \text{(2b)} \end{cases}.$$
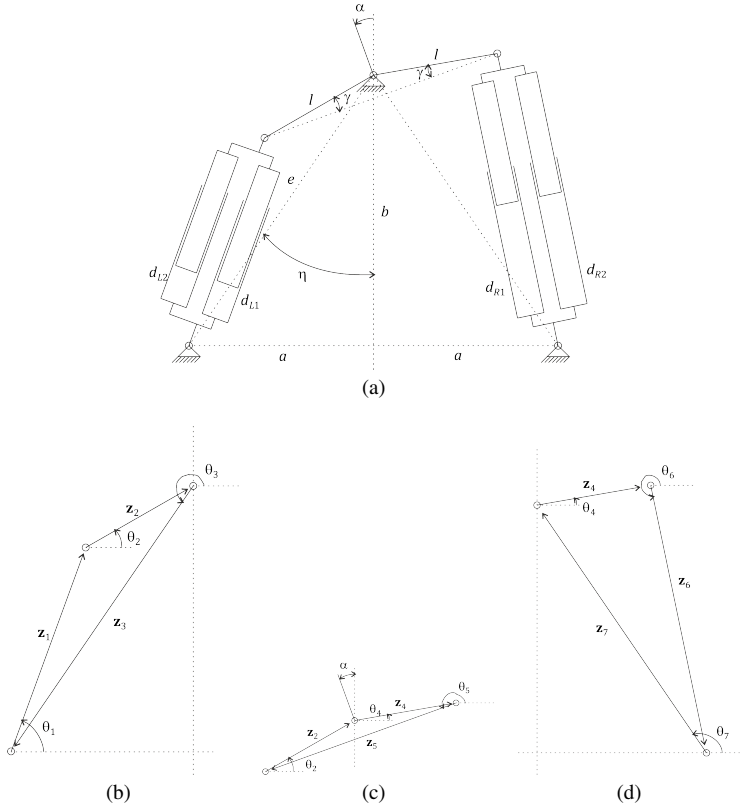
Fig. 3 (a) Schematic of the ground-steering sensing mechanism, where α is the steering angle of the nose gear, d_{L1}, d_{L2}, d_{R1}, d_{R2} are the LVDT sensor measurements and e, l, η, γ are the geometric model parameters. Kinematic diagrams of: (b) left arm; (c) centre arm; (d) right arm. (Source [4]).

Squaring and summing to each other equations (2a) and (2b) results in,

$$d_{Li}^2(\cos(\theta_1)^2 + \sin(\theta_1)^2) = l^2(\cos(\theta_2)^2 + \sin(\theta_2)^2) + a^2 + b^2 - 2la\cos(\theta_2) - 2lb\sin(\theta_2), \tag{3}$$

where the substitutions $z_1 = d_{Li}$, $z_2 = l$, $z_3\cos(\theta_3) = -a$ and $z_3\sin(\theta_3) = -b$ have been made. Equation (3) can thus be rewritten as,

$$d_{Li}^2 = l^2 + a^2 + b^2 - 2l\left[a\cos(\theta_2) + b\sin(\theta_2))\right]. \tag{4}$$

The centre arm is shown in figure 3(c). The direction of $\mathbf{z}_2$ can be expressed as,

$$\theta_2 = \alpha + \gamma, \tag{5}$$

where α is the angular position of the nose wheel and γ is the fixed angle given in table 1. Similarly, the direction of $\mathbf{z}_4$ is given by,

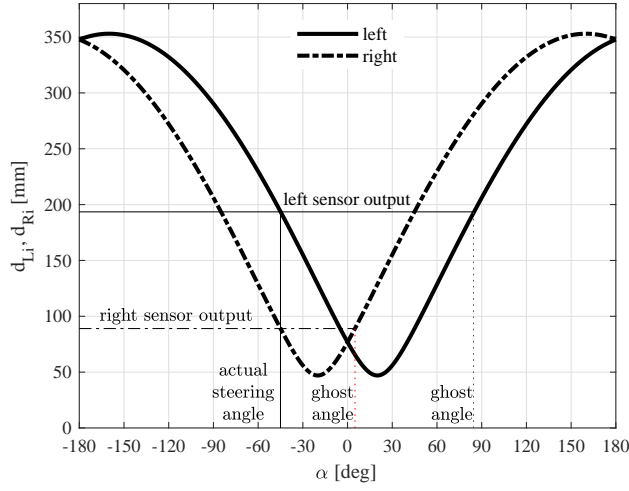$$\theta_4 = \alpha - \gamma. \tag{6}$$

Fig. 4 Position of the left (━━) and right (▪·▪·) sensors versus the nose wheel steering angle.

The closure equation of the right arm shown in figure 3(d) is obtained as follow,

$$\mathbf{z}_4 + \mathbf{z}_6 + \mathbf{z}_7 = \mathbf{0}, \tag{7}$$

which can be rewritten as,

$$\begin{cases} z_4\cos(\theta_4) + z_6\cos(\theta_6) + z_7\cos(\theta_7) = 0 & (8a) \\ z_4\sin(\theta_4) + z_6\sin(\theta_6) + z_7\sin(\theta_7) = 0 & (8b) \end{cases}.$$

Squaring and summing equations (8a) and (8b) results in,

$$d_{Ri}^2(\cos(\theta_6)^2 + \sin(\theta_6)^2) = l^2(\cos(\theta_4)^2 + \sin(\theta_4)^2) + a^2 + b^2 - 2la\cos(\theta_4) + 2lb\sin(\theta_4), \tag{9}$$

where the substitutions $z_6 = d_{Ri}$, $z_4 = l$, $z_7\cos(\theta_7) = -a$ and $z_7\sin(\theta_7) = b$ have been made. Hence, equation (9) becomes

$$z_6^2 = l^2 + a^2 + b^2 - 2l\left[a\cos(\theta_4) - b\sin(\theta_4))\right]. \tag{10}$$

As a result, the forward kinematic problem is determined by combining equations (4), (5), (6) and (10), which results in,

$$\begin{cases} d_{Li}^2 = l^2 + a^2 + b^2 - 2l\left[a\cos(\alpha + \gamma) + b\sin(\alpha + \gamma))\right] & (11a) \\ d_{Ri}^2 = l^2 + a^2 + b^2 - 2l\left[a\cos(\alpha - \gamma) - b\sin(\alpha - \gamma))\right] & (11b) \end{cases},$$

where the displacements of the left and right LVDTs (d_{Li}, d_{Ri}) can be calculated given the knowledge of the model parameters and the (known) true value of the steering angle α.

The nonlinear relationship between the LVDT displacements and the steering angle, given by equation (11), is shown in figure 4, with the solid line for the left sensors $d_{Li}(\alpha)$ and with the dash-dotted line for the right sensors $d_{Ri}(\alpha)$. $d_{Li}(\alpha)$ reaches a minimum at
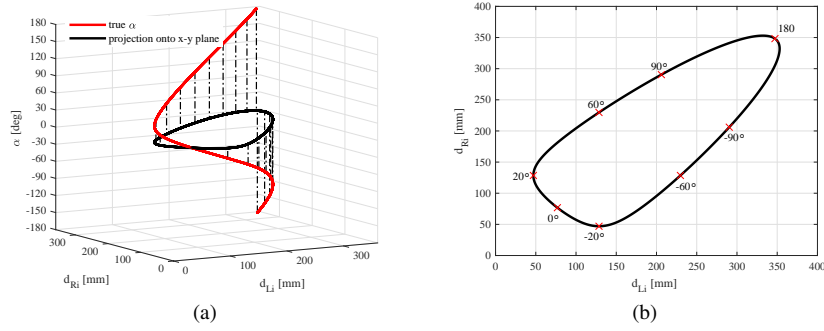
(a)   (b)

Fig. 5 (a) Variation of the steering angle with respect to the left and right sensor outputs. The true steering angle is shown with the red solid line (━━) and its projection to the x-y plane with the black solid line (━━). (b) Admissible sets of right and sensor displacements (d_{Ri}, d_{Li}); each set of right and left sensor output correspond to a unique value of the steering angle α. (Source [5]).

$\alpha = 20°$ meaning that it is a non-injective function in the interval $]-180°,\ 180°[$, hence not invertible. The same applies to $d_{Ri}(\alpha)$, which has a minimum at $\alpha = -20°$. It is important to notice, however, that even if the formulation has been derived for the full angular range, practical values of the aircraft steering angle during taxi are considered in the interval $]-90°,\ 90°[$.

As a consequence there is ambiguity associated with the steering angle estimate if only sensors on one side were to be used. As shown in figure 4, each individual sensor displacement could be generated by two distinct values of α, but only one of these two is the actual steering angle. Both the left and right sensor measurements must be used to determine the unique value of the actual steering angle.

Combining these sets of left and right sensor measurements with the actual steering angle generates a 3D relationship among these entities, which is shown with the red solid line in figure 5(a). This red line can be projected onto the x-y plane, which results in a manifold: the black solid line shown in figure 5(b). Each point on this curve relates an ideally-measured set of left and right sensor measurements to its unique steering angle value.

However, our interest is to solve the inverse kinematic problem, which requires the estimation of the actual steering angle $\hat{\alpha}$ given the measurements from two left and two right sensors (d_{Li}, d_{Ri}). To begin with we consider a deterministic scenario, in which the LVDT measurements are not affected by noise or faults and the model parameters are known precisely. As shown in [4], the system of equations (11) can be rewritten as,

$$\begin{cases} [a\cos(\alpha+\gamma)+b\sin(\alpha+\gamma))] = \dfrac{l^2+a^2+b^2-d_{Li}^2}{2l} & \text{(12a)} \\[2ex] [a\cos(\alpha-\gamma)-b\sin(\alpha-\gamma))] = \dfrac{l^2+a^2+b^2-d_{Ri}^2}{2l} & \text{(12b)} \end{cases}$$

which results in,

$$\begin{cases} \sin(\alpha)\left[b\cos(\gamma) - a\sin(\gamma)\right] + \cos(\alpha)\left[a\cos(\gamma) + b\sin(\gamma)\right] - \dfrac{l^2 + a^2 + b^2 - d_{Li}^2}{2l} = 0 \\ \sin(\alpha)\left[a\sin(\gamma) - b\cos(\gamma)\right] + \cos(\alpha)\left[a\cos(\gamma) + b\sin(\gamma)\right] - \dfrac{l^2 + a^2 + b^2 - d_{Ri}^2}{2l} = 0 \end{cases}$$

$$\text{(13a)}$$

$$\text{(13b)}$$

and given a set of (d_{Li}, d_{Ri}), the steering angle could be found iteratively solving equations (13a) and (13b), using for example Newton-Raphson method [4]. However, the iterative method described in [4] might require expensive and time consuming computations, and hence a closed-form solution is sought in this paper.

The right-hand members of equations (12a) and (12b) can be defined as,

$$L_i \triangleq \frac{l^2 + a^2 + b^2 - d_{Li}^2}{2l}, \ R_i \triangleq \frac{l^2 + a^2 + b^2 - d_{Ri}^2}{2l}. \tag{14}$$

Substituting equations (14), (5) and (6) into equations (12a) and (12b) gives,

$$\begin{cases} a\cos(\theta_2) + b\sin(\theta_2) = L_i & \text{(15a)} \\ a\cos(\theta_4) - b\sin(\theta_4) = R_i & \text{(15b)} \end{cases}$$

which can be solved independently. In solving equation (15a) we make use of the trigonometric identities

$$\sin(\theta_2) = 2\sin\left(\frac{\theta_2}{2}\right)\cos\left(\frac{\theta_2}{2}\right) = \frac{2\tan\left(\frac{\theta_2}{2}\right)}{1 + \tan^2\left(\frac{\theta_2}{2}\right)} \tag{16}$$

and

$$\cos(\theta_2) = \cos^2\left(\frac{\theta_2}{2}\right) - \sin^2\left(\frac{\theta_2}{2}\right) = 1 - 2\sin^2\left(\frac{\theta_2}{2}\right) = \frac{1 - \tan^2\left(\frac{\theta_2}{2}\right)}{1 + \tan^2\left(\frac{\theta_2}{2}\right)}. \tag{17}$$

Introducing a change of variable,

$$x \triangleq \tan\left(\frac{\theta_2}{2}\right) ; \quad \theta_2 \triangleq 2\arctan(x), \tag{18}$$

the trigonometric identities of equations (16) and (17) become,

$$\sin(\theta_2) = \frac{2x}{1 + x^2} ; \quad \cos(\theta_2) = \frac{1 - x^2}{1 + x^2}. \tag{19}$$

Substituting equation (19) into equation (15a) gives,

$$a\left(\frac{1 - x^2}{1 + x^2}\right) + b\left(\frac{2x}{1 + x^2}\right) - L_i = 0, \tag{20}$$

and results in the following second-order equation,

$$(L_i + a)x^2 - 2bx + (L_i - a) = 0, \tag{21}$$

which has two roots that can be calculated as,

$$x_{1,2} = \frac{2b \pm \sqrt{4b^2 - 4(L_i + a)(L_i - a)}}{2(L_i + a)} = \frac{b \pm \sqrt{a^2 + b^2 - L_i^2}}{L_i + a}. \tag{22}$$

Reapplying the change of variables of equation (18) to equation (22) gives the closed-form solutions of the steering angle estimates based on the left LVDT outputs as,

$$\alpha_{Li:1,2} = 2\arctan\left(\frac{b \pm \sqrt{a^2 + b^2 - L_i^2}}{L_i + a}\right) - \gamma. \tag{23}$$

Applying the same procedure to equation (15b) gives the following solution for the right LVDT outputs,

$$\alpha_{Ri:1,2} = 2\arctan\left(\frac{-b \pm \sqrt{a^2 + b^2 - R_i^2}}{R_i + a}\right) + \gamma. \tag{24}$$

A majority voting approach could be used to determine the final estimate from the two individual solutions of equations (23) and (24). In practice, however, the model parameters are subject to uncertainties and the LVDT measurements are noisy and potentially faulty. So alternative estimation algorithms have been considered, which are presented in the next two sections.

3 Virtual sensing using least-squares based estimation methods

This estimation method is motivated by an analogy with another overdetermined problem; the Global Positioning System (GPS). A GPS receiver obtains the transmitted signals from several orbiting satellites and calculates its position on Earth, which is then pointed out on a built-in map. The minimum number of satellites for the GPS receiver to calculate its position is 4 (the three coordinates and the clock offset between receiver and satellites), however, the receiver can usually track five or more satellites simultaneously. This means that there are more measurements than unknown, i.e. an overdetermined problem. The approach that is used in the GPS system to solve the overdetermined problem is a least-squares method [11–17].

Following this approach for the ground-steering system case study, equation (13), with the inclusion of uncertainties, can be expressed in a matrix form as [5],

$$\mathbf{A}\hat{\mathbf{x}} = \mathbf{d} - \hat{\mathbf{v}}, \tag{25}$$

where $\mathbf{A}$ is the the design matrix, which contains the model parameters only, $\hat{\mathbf{x}}$ is the unknown state vector, $\mathbf{d}$ is the measurement vector, and $\hat{\mathbf{v}}$ is the error vector, which represents the measurement noise, model errors and any sensor faults. The complete formulation for the Ordinary Least-Squares (OLS) estimator including the detailed description of each matrix appearing in equation (25) can be found in [5], where this method was first introduced. In this paper the OLS algorithm is briefly summarised as follows,

- Calculate the design matrix $\mathbf{A}$.
- Calculate the measurement vector $\mathbf{d}$ from the measured sensor signals.
- Compute the best estimate of α in the least-squares sense as,

$$\hat{\mathbf{x}} = \left(\mathbf{A}^T\mathbf{A}\right)^{-1}\mathbf{A}^T\mathbf{d}. \tag{26}$$

- We define the consistency of the estimation as,

$$\lambda = 1 - |\hat{\mathbf{x}}^T\hat{\mathbf{x}} - 1|. \tag{27}$$

- A fault is detected and isolated if $\lambda < 0.9$ but excluding any of the sensors from the estimation algorithm leads to a consistency index that is closer to 1.

A different technique for fault detection and isolation is the parity space approach [18–20]. However, the parity space approach is based on the assumption that the error vector has zero mean $E(\mathbf{v}) = 0$ and $E(\mathbf{v}\mathbf{v}^T) = \sigma\mathbf{I}$. In this particular case study, however, a Gaussian distribution of the sensor outputs does not correspond to a Gaussian distribution of the observation vector $\mathbf{d}$ because of the nonlinearity. This can be a reason why the parity space approach is not suited for fault detection and isolation in this application.

The OLS estimator is computationally inexpensive and provides accurate enough estimates with noisy measurements. It is shown in section 5, however, that it lacks robustness in the presence of larger deviations or faults in the sensors. This motivates least-squares estimation algorithms that are more robust against outliers. As presented in [5], M-estimators have higher tolerance for outliers with respect to OLS estimators. The cost function in this case is given by $\sum_{i=1}^{n}\rho(e_i)$, where $\rho(\cdot)$ is some function of the error e between the true and the estimated steering angles [21]. The solution is found via an iterative approach called iteratively reweighted least squares (IRLS), which is detailed in [5] and can be summarised as follows:

- Select an initial estimate, which can be the median estimate for example;
- At each iteration calculate the error residuals e_i and associate weights from the previous iteration;
- Solve for the new weighted least-squares estimate,

$$\hat{\alpha} = \left(\mathbf{H}^T\mathbf{W}\mathbf{H}\right)^{-1}\mathbf{H}^T\mathbf{W}\hat{\alpha} \tag{28}$$

where $\hat{\alpha}$ is a vector containing all candidate solutions, $\mathbf{H} \in \mathfrak{R}^{8\times1}$ is a scaling vector, and $\mathbf{W}$ is a diagonal matrix containing the weights;
- Repeat the previous two steps until convergence.

Different weighting functions can be used to determine matrix $\mathbf{W}$ used in equation (28). In this paper the Huber objective function [21] is used, which results in,

$$w(e_i) = \begin{cases} 1 & |e_i| \leq k \\ k/|e_i| & |e_i| \leq k \end{cases}, \tag{29}$$

where k is a tuning constant, which has been chosen to be twice the median absolute deviation $\mathrm{MAD} = \mathrm{med}_i|\alpha_i - \mathrm{med}_j\alpha_j|$ in this study, where $\mathrm{med}_j\alpha_j$ is the median of the observations. The smaller the value of k, the more the estimator is resistant to outliers. Although efficient to detect outliers, the IRLS is not always able to deal with the presence of sensor faults, as shown in section 5. A different approach for the estimation of the steering angle is the soft-computing (S-C), or soft-voting, method, which is presented in the next section.
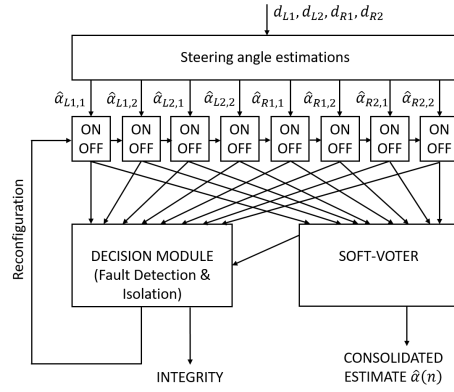
Fig. 6 Soft-voting estimation algorithm that uses a monitoring scheme to exclude faulty sensors.

4 Virtual sensing using a soft-computing approach

The soft-computing (S-C) approach is a sensor management technique that is similar to the majority voting approach, but in this case the observations are assigned weights that are based on fuzzy membership functions and the final estimate is computed as a weighted average of all valid observations [8,7]. The fuzzy membership functions are also used to assign an amount of trust to each valid observation. The soft-voting algorithm is implemented as illustrated in figure 6:

- The steering angle estimation signals, calculated using equations (23) and (24), are used simultaneously in two distinct modules, as introduced in section 1: the soft-voter module, which is used for the calculation of the final consolidated estimate, and the decision (or monitoring) module, which is used for the calculation of the integrity level and the fault detection and isolation. If a fault in one of the sensors is declared by the decision module, then the reconfiguration path switches off the corresponding sensor, as indicated by the ON/OFF elements in figure 6.
- In the soft-voter module each valid signal is assigned a weight and the consolidated estimated steering angle is the weighted average of the individual signals,

$$\hat{\alpha} = \sum_{i=1}^{n} w_i \hat{\alpha}_i, \tag{30}$$

where w_i denotes the weight assigned to the ith input signal $\hat{\alpha}_i$ and n denotes the number of valid sensors. $\hat{\alpha}_i$ is given by equations (23, 24);
- The weight w_i used here depends on the membership degree, which is calculated from a membership function. There exists many types of membership functions, for example: triangular, trapezoidal, Gaussian, two sided Gaussian plus a flat top, sigmoidal, and polynomial. The one used here and represented in figure 7 is the product of two sigmoidal membership functions that are expressed as,

$$\mu_i(\hat{\alpha}, \hat{\alpha}_i) = \frac{1}{1 + e^{-a_1[(\hat{\alpha} - \hat{\alpha}_i) - c_1]}} \cdot \frac{1}{1 + e^{-a_2[(\hat{\alpha} - \hat{\alpha}_i) - c_2]}}, \tag{31}$$

where the parameters a and c have been selected as $a_1 = 4$, $c_1 = -2$, $a_2 = -4$ and $c_2 = 2$.

– The weight is calculated as,

$$w_i = \frac{\mu_i}{\sum_{j=1}^{n} \mu_j}, \qquad (32)$$

where $0 \leq \mu_i \leq 1$. The computation of the membership degree μ_i is illustrated in figure 7.
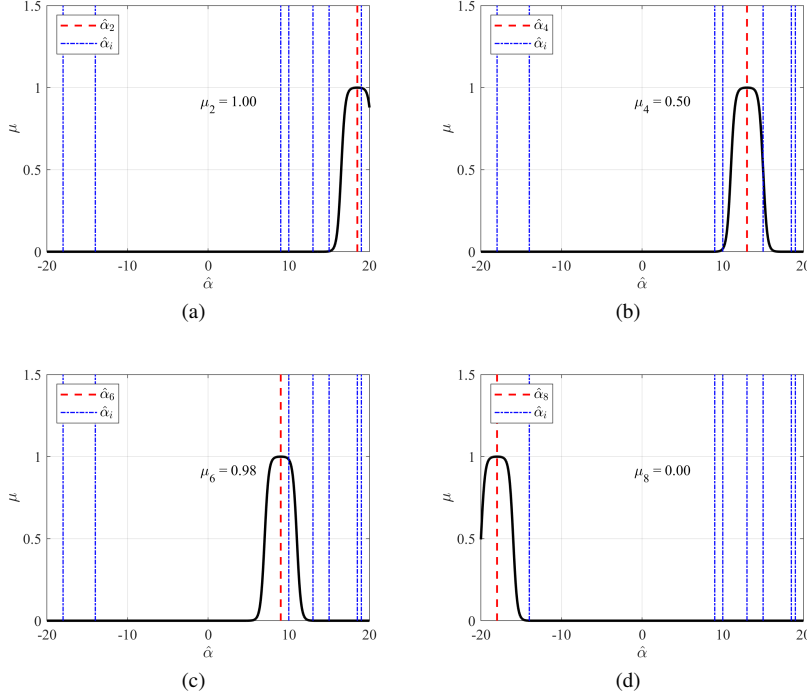

Fig. 7 Examples of soft-voting operation. The membership function is shown with the black solid line (▬▬), the current value of each sensor signal is shown with the red dashed line (▬ ▬ ▬), whereas the remaining valid sensor signals are shown with the blue dash-dotted line (▬·▬·). The current value of each sensor signal forms the centre of its membership function. The membership degree of the current signal is determined by the largest membership degree of the remaining valid signals.

– The current value of each signal forms the centre of its corresponding membership function. The membership degree for this signal is the largest membership degree of the remaining valid signals according to this "membership function",

$$\mu_i = \max_{i \neq j} \mu_i(\hat{\alpha}_j - \hat{\alpha}_i). \qquad (33)$$

For example, the membership degree of signal two in figure 7(a) is 1 because the next closest signal crosses its membership function on the top flat part. The membership degree of signal four in figure 7(b) instead, is 0.5 because the next closest signal crosses the membership function on its shoulder at that level. Similarly, the membership degrees of all remaining valid signals can be obtained following the same procedure.
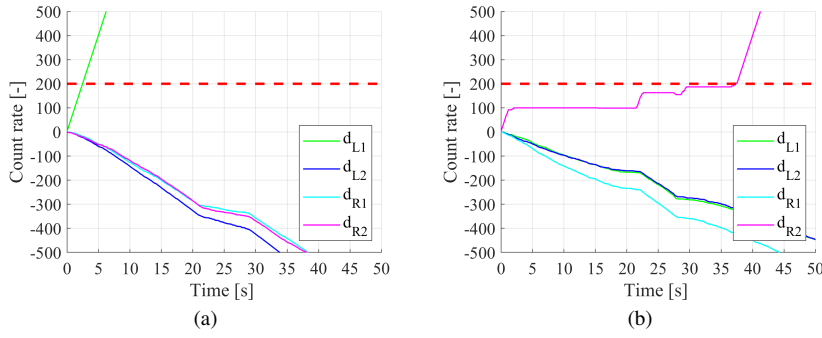
Fig. 8 Examples of monitoring operation. (a) Hard fault on sensor d_{L1} (locked); (b) Small constant bias on sensor d_{R2}. The monitoring count rates for the sensors d_{L1}, d_{L2}, d_{R1}, d_{R2} are shown with the green (━━), blue (━━), cyan(━━) and magenta (━━) lines, respectively. Sensor faults are detected and corresponding sensor signals are switched off once the count rate of the sensor crosses the threshold, which is shown with the dashed red line (━ ━ ━).

- In the decision module, the "count rate" ξ of the ith signal is calculated at each iteration according to its corresponding membership degree μ_i:

$$\text{If } \mu_i = 1 \text{ then } \xi_i = -1 \tag{34a}$$

$$\text{If } 0 \le \mu_i \le 1 \text{ then } \xi_i = 0, \tag{34b}$$

$$\text{If } \mu_i = 0 \text{ then } \xi_i = +2 \tag{34c}$$

- If the count rate goes beyond a threshold, for example $\bar{\xi} = 200$ over a certain period of time, the corresponding sensor is declared faulty and its contribution to the consolidated estimate is switched off. For example, figure 8(a) shows the count rate, at 100Hz, of the sensor condition during a test in which the nose gear is steering from $-150°$ to $150°$ at a rate of $30°$ every 5 seconds and the sensor d_{L1} is subject to a hard fault. The soft-computing algorithm quickly detects the anomaly with sensor d_{L1} (green line) and when its count rate crosses the threshold (red dashed line) at around 2.5s the sensor is declared invalid and taken out from future estimations. Similarly, figure 8(b) shows the count rate of the sensor condition during the same test as before, but with sensor d_{R2} subject to a small bias fault instead of the hard fault on d_{L1}. In this case the algorithms take longer (around 37.5s) to declare the sensor invalid, as subtle faults are more difficult to detect. In practical implementations, it is important to introduce a saturation limit on the lower value of the count rates. This serves the purpose of avoiding that the count rate of a sensor keeps decrementing indefinitely until it reaches very large negative values, affecting the performance of the fault detection should a fault occur, since a large time interval would be needed before the count rate increases to overtake the upper threshold.
- The count rate of the ith sensor signal becomes positive when the corresponding weight in the voted signal is equal to zero ($w_i = 0$), therefore no transients occur once the failure is declared on the ith sensor and the corresponding signal is switched off. This soft-voting approach is thus similar to a majority voting approach, but in the soft-voting approach the contribution of a faulty signal is reduced instead of being ruled out.

– The integrity of the estimate is calculated as the average level of trust of all sensors,

$$\psi = \frac{\sum \max \mu_{d_i}}{4}.$$

(35)

where μ_{d_i} is the ith membership degree for each sensor.

5 Simulation results

In this section the OLS and IRLS methods are compared with the S-C method for several scenarios in which the digital twin of the ground-steering system is subject to model uncertainties, measurement noise and sensor faults.

When these unknown inputs are considered, the eight steering angle estimates given by equations (23) and (24) become,

$$\hat{\alpha}_{Li:1,2} = 2\arctan\left(\frac{\tilde{b} \pm \sqrt{\tilde{a}^2 + \tilde{b}^2 - \tilde{L}_i^2}}{\tilde{L}_i + \tilde{a}}\right) - \tilde{\gamma},$$

(36)

and

$$\hat{\alpha}_{Ri:1,2} = 2\arctan\left(\frac{-\tilde{b} \pm \sqrt{\tilde{a}^2 + \tilde{b}^2 - \tilde{R}_i^2}}{\tilde{R}_i + \tilde{a}}\right) + \tilde{\gamma},$$

(37)

where $\tilde{a} \in [a - \Delta, \ a + \Delta]$, $\tilde{b} \in [b - \Delta, \ b + \Delta]$, $\tilde{l} \in [l - \Delta, \ l + \Delta]$ and $\tilde{\gamma} \in [\gamma - \Delta_\gamma, \ \gamma + \Delta_\gamma]$. Δ and Δ_γ are the model uncertainties, which describe the error bounds of the model parameters. In this study Δ has been set to 2mm and Δ_γ set to $2°$. The variables $\tilde{L}_i$ and $\tilde{R}_i$ in equations (36) and (37) are defined as,

$$\tilde{L}_i \triangleq \frac{\tilde{l}^2 + \tilde{a}^2 + \tilde{b}^2 - \tilde{d}_{Li}^2}{2\tilde{l}}, \ \tilde{R}_i \triangleq \frac{\tilde{l}^2 + \tilde{a}^2 + \tilde{b}^2 - \tilde{d}_{Ri}^2}{2\tilde{l}},$$

(38)

where

$$\tilde{d}_{Li} = \sigma_s(1 + \varepsilon_s)\tilde{d}_{Lni} + d_{Lf},$$

(39)

and

$$\tilde{d}_{Ri} = \sigma_s(1 + \varepsilon_s)\tilde{d}_{Rni} + d_{Rf},$$

(40)

in which σ_s and ε_s are variables that depend on the type of fault, and $\tilde{d}_{Lni} \in [d_{Li} - \Delta_d, \ d_{Li} + \Delta_d]$ and $\tilde{d}_{Rni} \in [d_{Ri} - \Delta_d, \ d_{Ri} + \Delta_d]$, where Δ_d, which is set to 2mm, is the measurement error.

Equations (39) and (40) model a sensor fault as a discrepancy between the actual output of the system $\tilde{d}_{Lni}$, $\tilde{d}_{Rni}$ and the sensor output $\tilde{d}_{Li}$, $\tilde{d}_{Ri}$. Four generic types of faults, common to most sensors, are described: bias (offset), drift (linear or not), scaling (gain, linear, or not), hard fault (loss or locking of signal). The value of fault parameters σ_s, ε_s, d_{Lf} and d_{Rf} appearing in equations (39) and (40) for these different types of fault are indicated in table 2.

Severe faults, as for example the loss of signals, are generally easy to detect since a built-in test is generally provided by sensor manufacturers. This is why small anomalies like bias, small drift, etc. that are more difficult to recognise should be the focal point of a fault

Table 2 Model parameters for sensor faults.

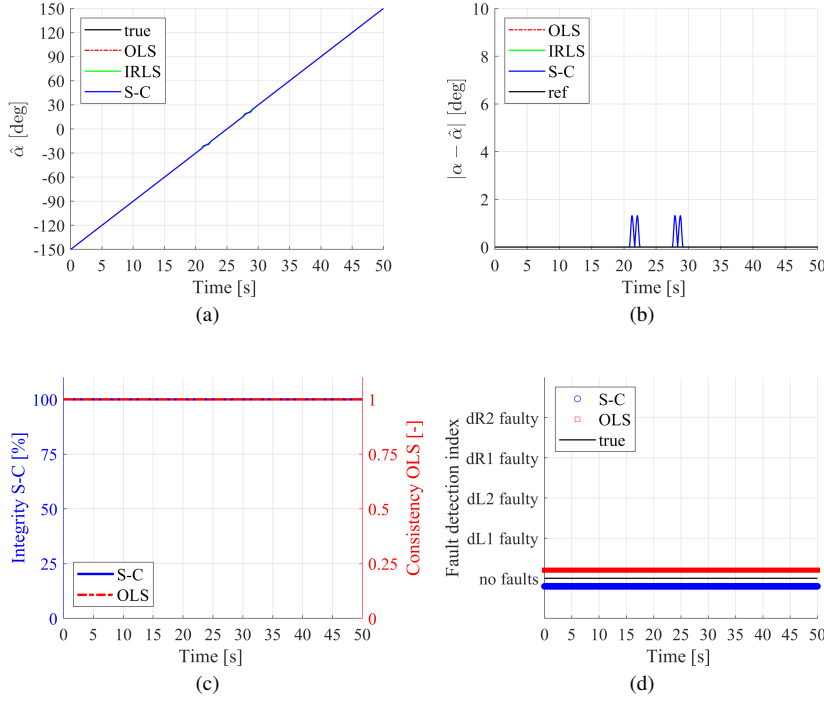|	Bias	Drift	Scaling	Hard fault	No fault
ε_s	0	0	$\neq 0$	0	0
σ_s	1	1	1	0	1
d_{Lf}, d_{Rf}	$\neq 0$ (const.)	$\neq 0$ (time varying)	0	const.	0

Fig. 9 Simulation results for case A, in which there is no model uncertainty, measurement noise and sensor faults. Black line (▬) for the true reference signal; red dash-dotted line (▪▪▪) for the OLS; solid green line (▬) for the IRLS and solid blue line (▬) for the S-C method. (a) Steering angle estimate; (b) Estimation accuracy; (c) Integrity for the S-C method and consistency for the OLS method according to equations (35) and (27); (d) Decision on fault detection and isolation.

detection and isolation module.

The true steering angle has been simulated as a ramp signal starting at -150° and increasing by 30° every 5 seconds, reaching 150° at 50 seconds.

The OLS, IRLS and S-C algorithms have been tested for the following scenarios:

– Case A:

Ideal scenario: no measurement noise, no parameter uncertainty and no faults. The results are shown in terms of estimated steering angle, estimation accuracy, integrity and fault detection and isolation in figure 9.
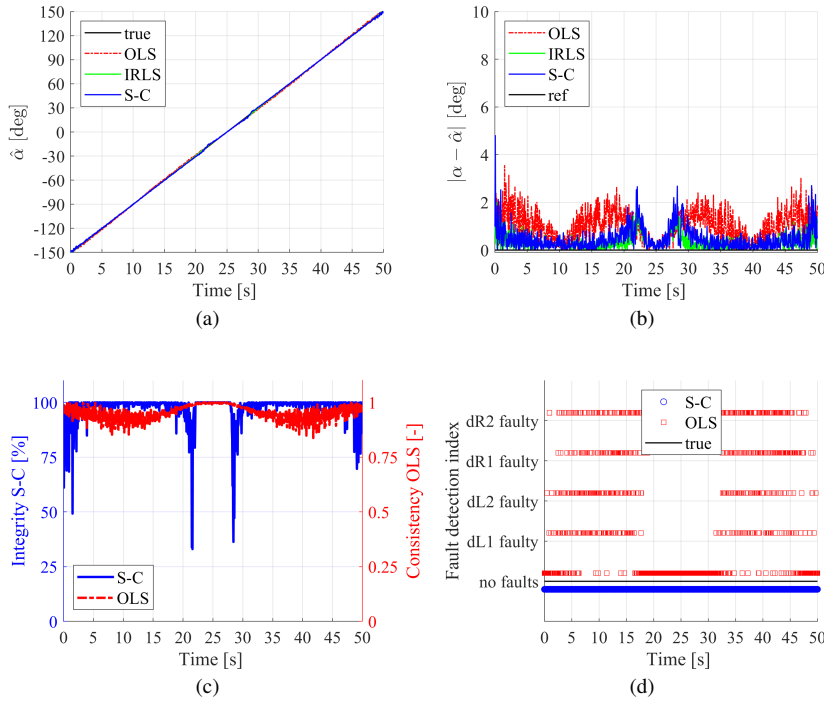
Fig. 10 Simulation results for case B that includes model uncertainty and measurement noise, but doesn't include any sensor faults. Black line (━━) for the true reference signal; red dash-dotted line (▪▪▪) for the OLS; solid green line (━━) for the IRLS and solid blue line (━━) for the S-C method. (a) Steering angle estimate; (b) Estimation accuracy; (c) Integrity for the S-C method and consistency for the OLS method according to equations (35) and (27); (d) Decision on fault detection and isolation.

All of the algorithms are able to accurately predict the steering angle in this ideal scenario, as shown in figures 9(a) and 9(b). The small errors given by the S-C method around $-20°$ and $20°$ visible in figure 9(b) are due to the flat top region of the membership function shown in figure 7. Both integrity and consistency are at maximum in this scenario, as shown in figure 9(c) and the fault detection index given in figure 9(d) reports no faults, as expected for the OLS and S-C. There is no obvious way of calculating the integrity or fault detection index for the IRLS.

– <u>Case B:</u>

Figure 10 shows the results of a simulation without faults, but with parameter uncertainty Δ set to 2mm and Δ_γ set to $2°$ and with measurement noise Δ_d set to 2mm.

The IRLS and S-C algorithms slightly outperform the OLS algorithm in terms of accuracy in this case as shown in figure 10(b). Although the OLS methods give a high consistency level (figure 10(c)) compared to the S-C method, it also detects a number of false positives for the fault detection and isolation, as shown in figure 10(d), even though none of the sensors is faulty .
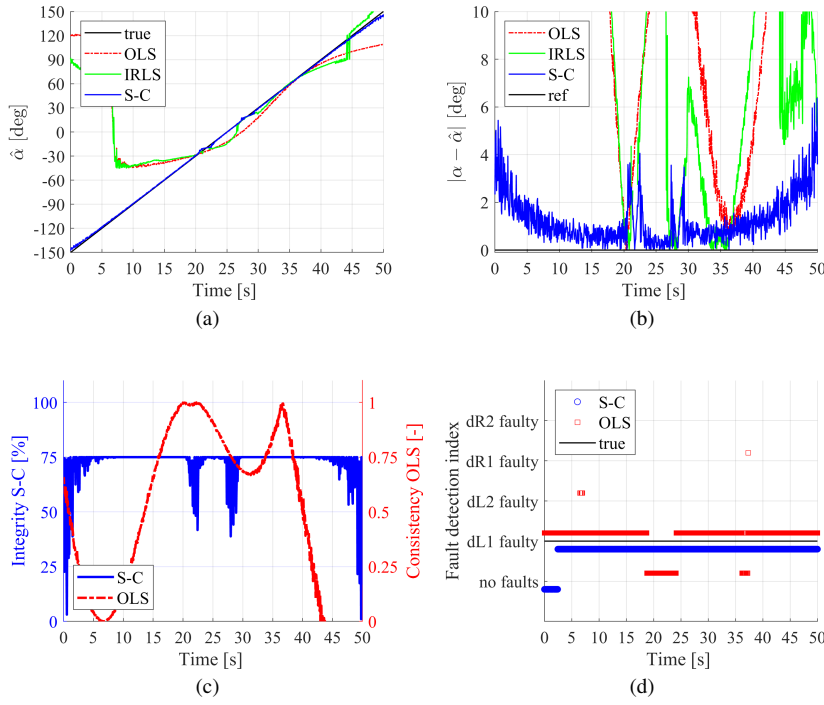
– <u>Case C:</u>

(a)

(b)

(c)

(d)

Fig. 11 Simulation results for case C that includes model uncertainty and measurement noise and a faulty sensor: hard fault on d_{L1}. Black line (━━) for the true reference signal; red dash-dotted line (■·■·) for the OLS; solid green line (━━) for the IRLS and solid blue line (━━) for the S-C method. (a) Steering angle estimate; (b) Estimation accuracy; (c) Integrity for the S-C method and consistency for the OLS method according to equations (35) and (27); (d) Decision on fault detection and isolation.

Figure 11 shows the results of the simulation with parameter uncertainty Δ set to 2mm and Δ_γ set to 2°, measurement noise Δ_d set to 2mm and a faulty sensor d_{L1} stuck at 150 mm, which is a hard fault.

This case of severe fault illustrates how the S-C is more robust than the LS based estimators. As shown in figures 11(a) and 11(b), the error of the estimation given by the S-C algorithm remains small, while the errors of the LS base estimators occasionally go out of scale. In figure 11(c) the integrity of the OLS is very low some of the time, whereas the integrity of the S-C approach is consistently to around 75%, indicating the loss of a sensor. This is verified by figure 11(d), which shows how quickly the S-C method realises that d_{L1} is faulty. It should be noted that also in this occasion the LS methods give false positives as well as no detections indicating that they are less reliable in performing FDI operations than the S-C approach.

– Case D:

Figure 12 shows the results of the simulation with parameter uncertainty Δ set to 2mm and Δ_γ set to 2°, measurement noise Δ_d set to 2mm and a faulty sensor $\tilde{d}_{R2} = \tilde{d}_{Rn2} + 15$ mm, which is a bias fault.
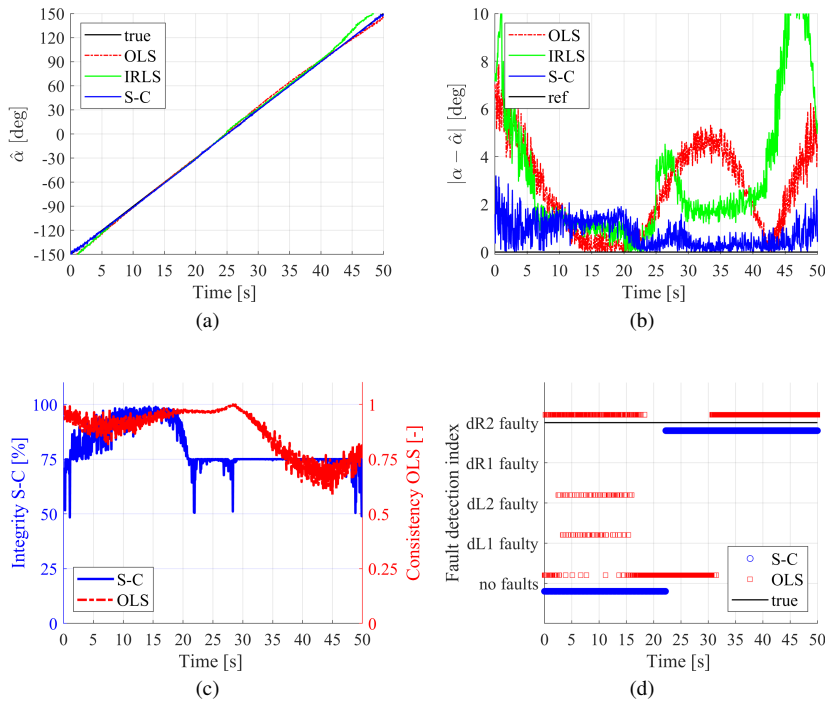
Fig. 12 Simulation results for case D that includes model uncertainty and measurement noise and a faulty sensor: small bias on d_{R2}. Black line (━) for the true reference signal; red dash-dotted line (▬·▬·) for the OLS; solid green line (━) for the IRLS and solid blue line (━) for the S-C method. (a) Steering angle estimate; (b) Estimation accuracy; (c) Integrity for the S-C method and consistency for the OLS method according to equations (35) and (27); (d) Decision on fault detection and isolation.

This case of milder fault is more difficult to detect when compared to the previous case of a severe fault because the faults might be mistaken for uncertainties and vice-versa. The S-C approach is still the most accurate and robust algorithm when compared with the LS based estimators, as shown in figures 12(a) and 12(b). Figure 12(c) shows that the integrity is initially estimated by the S-C algorithm to be around 100%, before dropping to levels below 75% meaning that the S-C algorithm needed some time before declaring one of the sensors as faulty as also shown in 12(d). This did not compromise the accuracy of the estimation, however, and the fault detection was still slightly quicker than that of the OLS.

6 Conclusions

In this paper the robust estimation of wheel direction in a ground-steering system for aircraft has been presented when using remote and redundant LVDT measurements that are subject to uncertainties and faults. This is used as an example of virtual sensing in a safety-critical application. The observational digital twin of the ground-steering system consists of a kinematic model of the sensing mechanism together with unknown inputs such as the

model uncertainties, the measurement noise and the potential sensor faults. Because of these effects, and also the nonlinear arrangement of the sensors, the angle estimates from each of the sensors are different from each other, and it is important to not only reliably estimate the controlled signal under these conditions, but also to assess the degree of confidence with which the estimate should be treated. The forward kinematic problem, which was first solved in [4], has been summarised in section 2, whereas the inverse kinematic problem has been solved in closed-form in this paper. The resulting nonlinear relationship between the steering angle and the sensor outputs was also investigated.

Three distinct estimation algorithms have been compared for the estimation of the wheel direction in presence of model uncertainties, measurement noise and sensors faults. Two of these algorithms, which were already presented in [5] are least-squares based approaches, namely ordinary least squares (OLS) and iteratively reweighted least squares (IRLS). The other approach, which was only introduced in [5], but formulated and described in detail in this paper, is called soft-computing (S-C) and is based on fuzzy logic techniques. The three methods have been compared in different scenarios where uncertainties, noise and different types of sensor faults have been included. The algorithms have been tested not only in terms of estimation accuracy, but also ability of detecting and isolating faults.

A metric for the estimation integrity has also been introduced as a measure of the amount of trust with which the final estimate is credited. It is shown that the S-C estimation algorithm is more robust than the LS based methods in the presence of uncertainties and sensor faults. Overall, the S-C algorithm demonstrates a higher accuracy and better fault detection and isolation decisions when compared to the LS methods.

Conflict of interest

The authors declare that they have no conflict of interest.

References

1. N.S. Currey, *Aircraft Landing Gear Design: Principles and Practices*. AIAA Education Series (American Institute of Aeronautics and Astronautics, Washington, DC, USA, 1988). DOI 10.2514/4.861468
2. Federal Aviation Administration, *Aviation Maintenance Technician Handbook-Airframe (Chapter 13)*, vol. 2 (United States Department of Transportation, Oklahoma City, OK, USA, 2018)
3. D.W.S. Young, B. Ohly, SAE Transactions **94**, 881 (1985). DOI 10.4271/851940
4. M. Dal Borgo, S.J. Elliott, M. Ghandchi Tehrani, I.M. Stothers, in *Proceedings of the 26th International Congress on Sound and Vibration (ICSV26)* (Canadian Acoustical Association, Montreal, Canada, 2019), pp. 1–8
5. M. Dal Borgo, S.J. Elliott, M. Ghandchi Tehrani, I.M. Stothers, in *Proceedings of the 38th IMAC, A Conference and Exposition on Structural Dynamics 2020*, vol. 3, ed. by Z. Mao (Springer, Cham, Houston, TX, USA, 2020), vol. 3, pp. 107–118. DOI 10.1007/978-3-030-47638-0_12
6. H.V.M. Catapult. Feasibility of an immersive digital twin (2018). Accessed: 2019-11-29
7. D. Berdjag, A. Zolghadri, J. Cieslak, P. Goupil, in *Conference on Control and Fault-Tolerant Systems (SysTol)* (Nice, France, 2010), pp. 137–142. DOI 10.1109/SYSTOL.2010.5675993
8. M. Oosterom, R. Babuska, H.B. Verbruggen, IEEE Transactions on Systems, Man, and Cybernetics, Part C (Applications and Reviews) **32**(2), 125 (2002). DOI 10.1109/TSMCC.2002.801357

9. J. Marzat, H. Piet-Lahanier, F. Damongeot, E. Walter, Proceedings of the Institution of Mechanical Engineers, Part G: Journal of Aerospace Engineering **226**(10), pp 1329 (2012). DOI 10.1177/0954410011421717. URL https://hal-supelec.archives-ouvertes.fr/hal-00615617

10. M. Zhang, R.M. Jiang, H. Nie, International Journal of Aerospace Engineering (Article ID 1626015), 14 (2016). DOI 10.1155/2016/1626015

11. G. Blewitt, *Basics of the GPS technique: observation equations* (Swedish Land Survey, 1997), pp. 10–54

12. R.B. Langley, GPS World **2**(7), 45 (1991)

13. R.B. Langley, GPS World **10**(5), 52 (1999)

14. R.B. Langley, GPS World **10**(3), 60 (1999)

15. L. Heng, G. Gao, T. Walter, P. Enge, GPS World **22**(11), 44 (2011)

16. A. Oxley, *Uncertainties in GPS Positioning: A mathematical discourse*, 1st edn. (Academic Press, 2017)

17. D. Rutledge, GPS World **21**(5), 42 (2010)

18. T. Zhang, F. Wang, W. Fu, Applied Sciences **8**(6), 865 (2018). DOI 10.3390/app8060865

19. Y. Bo, Q. Yongyuan, C. Yan, Measurement Science and Technology **17**(6), 1522 (2006). DOI 10.1088/0957-0233/17/6/033

20. P.M. Frank, Automatica **26**(3), 459 (1990). DOI 10.1016/0005-1098(90)90018-D

21. P.J. Huber, E.M. Ronchetti, *Robust statistics* (John Wiley & Sons, 2009). DOI 10.1002/9780470434697